ARCHIVES OF ACOUSTICS
24, 3, 255–267 (1999)

# COMPLETE CHARACTERIZATION OF ULTRASOUND TRANSDUCERS THROUGH THE "FIELD II" SIMULATION PROGRAM

G. GUIDI and S. FALTERI

Electronic Engineering Department
University of Florence
(3–50139 Florence, Via S. Marta, Italy)
e-mail: g.guidi@ieee.org

Acoustic field characterization is usually limited to the measurement of the field amplitude, and employs well-known investigation methods. However, it is known that in many applications an important role is played by the phase field distribution. For example, a complete acoustic field characterization (i.e. the determination of both the amplitude and phase field distributions), results very useful for the correct interpretation of the Doppler signals detected by such a transducer. In this paper a technique for the measurement of the complex field (phasor) produced by single element transducers is presented. It is based on the time domain analysis of the RF pressure signals produced in front of the transducer. The technique, proposed as a general experimental procedure for the concurrent measurement of phase and amplitude fields, is here applied to fields synthesized with the "Field II" simulation program. Simulation results are compared with field distributions both available in the literature in analytic form, or derived experimentally.

## 1. Introduction

Important issues, like the quantitative assessment of pressure impinging on human tissues or the estimation of transducers' focusing properties, are yielded by estimating the field amplitude in front of the transducer face.

As known, such evaluation can be made with direct measurement, by scanning with hydrophones the volume of interest, or indirectly, by measuring the signal backscattered toward the transducer from a point-like target located at different places.

The former method is usually considered the "gold standard" for any quantitative estimation of pressure levels, while focusing properties, providing a target small enough to be considered like a point, can be detected with the latter too.

In any case the quantity to be measured is always the field amplitude, while little emphasis is given to the phase field distribution.

As a matter of fact, the phase can be neglected in imaging systems characterization, where the lateral resolution — or the capability to distinguish two near details along a line perpendicular to the beam axis at a certain range — is determined by the beam Full

Width at Half Maximum (FWHM), given as the intersection between the field *amplitude* at the range of interest, and a −6 dB threshold level [1].

When a beam has to be characterized for a Doppler equipment rather than an imager, *phase* field distribution becomes important [2, 3]. A scatterer traveling across an acoustic field, whose phase distribution differs from plane wave conditions, originates a frequency modulation in the backscattered signal which broadens the Doppler Spectrum with respect to the simple theoretical predictions associated to the transit-time only.

Beam characterization of transducers to be coupled to Doppler flowmeters should therefore take into account not only the amplitude but also the phase distribution with proper measurement techniques [4, 5].

In this paper a method for calculating the complex (amplitude and phase) spatial field from the time domain RF signals, as those detected from hydrophones, is presented. Despite of the fact that it was proposed as a general technique, it has been verified here on simulated RF signals. A comparison between simulated and experimental intensity beamplots, for two differently focused circular transducers, is finally shown.

## 2. Methods

The tool used for simulating the complex field distribution is the "Field II" program, developed by JENSEN [6], which employs the spatial impulse response method proposed by TUPHOLME and STEPHANISHEN [7, 8].

The original method requires to know the spatial impulse response of the transducer geometry; in order to reduce the analytic complexity involved, the simulation program provides the subdivision of the transducer surface in small squares, whose impulse response is known, and evaluates the global field by summing the response of each elementary radiator. The calculation time is kept low considering the small elementary square aperture, and using for this reason far-field approximation for each transducer element.

The simulator inputs define the transducer geometry as aperture shape and dimensions, focusing properties, possible presence of apodization, and the excitation signal applied to the transducer. As output it supplies the space-time properties of the pressure field $u(x, y, z, t)$ resulting from a known velocity $v(x, y, z, t)$ over the transducer surface. Such output is analogous to the RF signal displayed by an oscilloscope connected to an hydrophone located at the points of simulation.

In our experiments a spherically focused circular transducer was used, as the one sketched in Fig. 1, where the cartesian reference is also shown.

The excitation was chosen as a burst at frequency $f_0$ made by an integer number of pulses. The velocity distribution was supposed uniform over the whole transducer and given in the form:

$$v(t) = v_0 e^{i\omega_0 t}, \qquad \omega_0 = 2\pi f_0 \tag{1}$$

with $v_0$ unknown and set to an arbitrary value. However, since the scope of the work was not to simulate a transducer in order to guess an absolute amplitude value, but just for having a relative amplitude beam plot and the absolute phase distribution, the

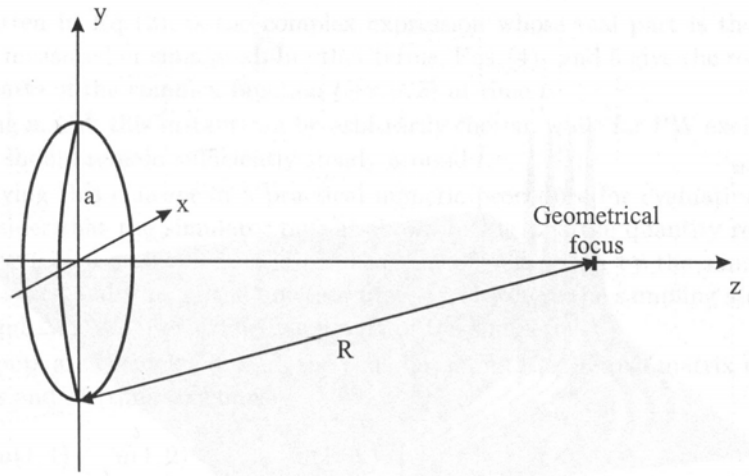


Fig. 1. Spherically focused circular transducer and reference system.

knowledge of $v_0$ was actually not required. For a quantitative simulation $v_0$ should be estimated, as for example in the work of MAIONE *et al.* [9], starting from the knowledge of the exciting amplitude, and simulating with PSpice and a proper electro-mechanical model the actual transducer vibration.

Figure 2 shows one of the typical outputs of the program. It was originated by simulating a circular transducer with a diameter of $2a = 8\,\text{mm}$, radius of curvature $R = 30\,\text{mm}$ (geometrical focus), operating at $f_0 = 8\,\text{MHz}$ with no apodization. The excitation signal was a narrowband pulse composed by 4 sinusoid cycles. The display shows the behavior in time of the field at 30 mm from the aperture, for several off-axis displacements. The time axis starts from an offset, supplied as output by the simulator, which represents the global delay of this space-time distribution respect to the application of the excitation to the transducer. By looking at the figure, it can be identified the pulse train proceeding and, for different time instants, it is possible to see the growing of sidelobes as the time passes.

A field representation in the time domain, as this one described above, is doubtlessly the best one for analyzing the effect of a transient excitation. On the other hand, when a beamplot have to be calculated, the most convenient representation is that where the time dependent term is separated by the space varying one. Indicating with $u(x, y, z, t)$ the behavior in time of the acoustic field at the spatial point $\{x, y, z\}$, for a CW excitation or a steady period of a pulsed excitation, the field can be expressed as:

$$u(x, y, z, t) = \text{Re}\left\{\underline{U}(x, y, z)e^{j\omega_0 t}\right\}, \tag{2}$$

where $\underline{U}(x, y, z)$ is the complex function obeying to the Helmoltz equation, which defines the spatial varying part of the field [10], having its own modulus and phase:

$$\underline{U}(x, y, z) = U(x, y, z)e^{j\phi(x,y,z)}. \tag{3}$$

Looking at $u(x, y, z, t)$ as the projection on the real axis of a rotating phasor with angular velocity $\omega_0$, if we consider a specific point $\{\tilde{x}, \tilde{y}, \tilde{z}\}$ at two specific times $\tilde{t}$ and $\tilde{t} - \Delta\tilde{t}$,

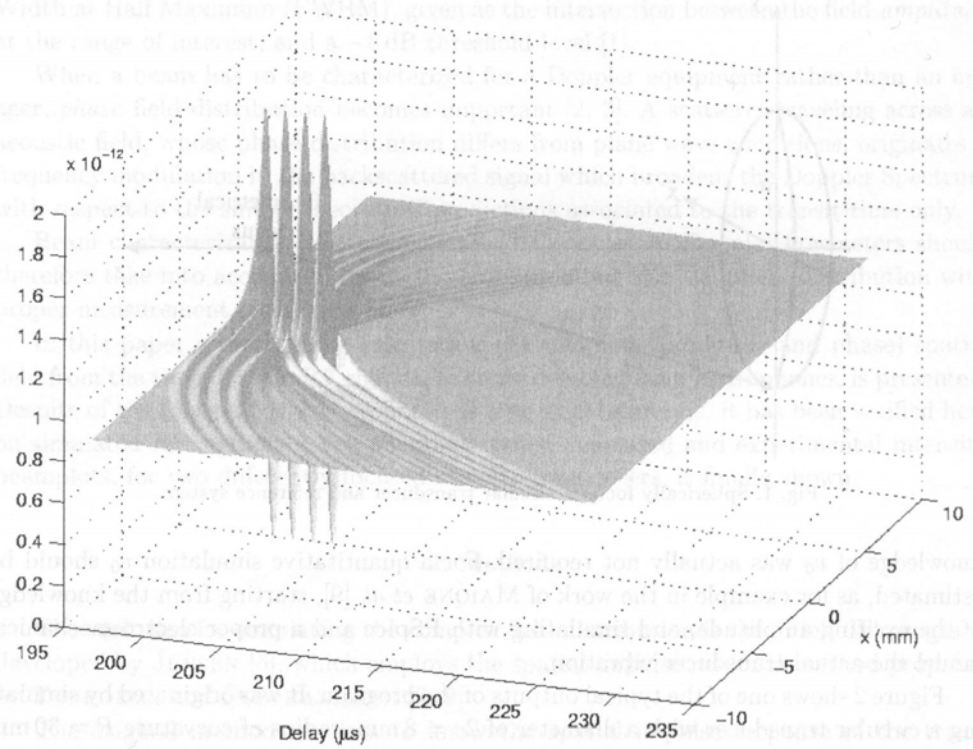


Fig. 2. Typical output of the "Field II" program, obtained for a Spherically focused circular transducer with $a = 4\,\text{mm}$ and $R = 30\,\text{mm}$, simulating the field generated at 30 mm from the transducer, for $y = 0$ and $x$ ranging from $-10$ and 10 mm.

the field can be written as:

$$\begin{aligned} u(\tilde{x},\tilde{y},\tilde{z},\tilde{t}) &= U(\tilde{x},\tilde{y},\tilde{z})\cos\left[\omega_0\tilde{t}+\phi(\tilde{x},\tilde{y},\tilde{z})\right], \\ u(\tilde{x},\tilde{y},\tilde{z},\tilde{t}-\Delta\tilde{t}) &= U(\tilde{x},\tilde{y},\tilde{z})\cos\left[\omega_0\tilde{t}-\omega_0\Delta\tilde{t}+\phi(\tilde{x},\tilde{y},\tilde{z})\right]. \end{aligned} \tag{4}$$

If $\Delta\tilde{t}$ is chosen such as:

$$\omega_0\Delta\tilde{t} = \frac{\pi}{2},$$

the expression $(4)_2$ becomes:

$$\begin{aligned} &u(\tilde{x},\tilde{y},\tilde{z},\tilde{t}-\Delta\tilde{t}) \\ &\quad = U(\tilde{x},\tilde{y},\tilde{z})\cos\left[\left(\omega_0\tilde{t}+\phi(\tilde{x},\tilde{y},\tilde{z})\right)-\frac{\pi}{2}\right] = U(\tilde{x},\tilde{y},\tilde{z})\sin\left[\omega_0\tilde{t}+\phi(\tilde{x},\tilde{y},\tilde{z})\right]. \end{aligned} \tag{5}$$

Hence combining Eq. $(4)_1$ and 5 as the real and imaginary part of a complex number, we have:

$$\begin{aligned} &u(\tilde{x},\tilde{y},\tilde{z},\tilde{t})+ju(\tilde{x},\tilde{y},\tilde{z},\tilde{t}-\Delta\tilde{t}) \\ &\qquad = U(\tilde{x},\tilde{y},\tilde{z})\cos\left[\omega_0\tilde{t}+\phi(\tilde{x},\tilde{y},\tilde{z})\right]+jU(\tilde{x},\tilde{y},\tilde{z})\sin\left[\omega_0\tilde{t}+\phi(\tilde{x},\tilde{y},\tilde{z})\right] \\ &\qquad = U(\tilde{x},\tilde{y},\tilde{z})e^{j\left[\omega_0\tilde{t}+\phi(\tilde{x},\tilde{y},\tilde{z})\right]} = \underline{U}(\tilde{x},\tilde{y},\tilde{z})e^{j\omega_0\tilde{t}} \end{aligned}$$

that, as written in Eq. (2), is the complex expression whose real part is the quantity hydrophone measured or simulated. In other terms, Eqs. $(4)_1$ and 5 give the real and the imaginary parts of the complex function $\underline{U}(\tilde{x}, \tilde{y}, \tilde{z})$ at time $\tilde{t}$.

Operating in CW this instant can be arbitrarily chosen, while for PW excitation the spatial field should remain sufficiently steady around $\tilde{t}$.

For applying this concept in a practical numeric procedure for evaluating $\underline{U}(\,)$, we have to consider that the simulator output shown in Fig. 2 is the quantity represented by Eq. (2) for $y = \tilde{y}$ and $z = \tilde{z}$. The resulting set of data given by the simulator is a sampling in space and time of the function $u(x, \tilde{y}, \tilde{z}, t)$, where the sampling steps over $x$ and $t$, $\Delta x$ and $\Delta t_s$, are user defined as inputs of the simulator.

The outputs are the delay $d$ of all the time-lines, and the 2D real matrix $\mathbf{u}$, with $M$ (space) rows and $N$ (time) columns:

$$\mathbf{u} = \begin{bmatrix} u(1,1) & u(1,2) & \dots & u(1,N) \\ u(2,1) & u(2,2) & \dots & u(2,N) \\ \vdots & \vdots & \vdots & \vdots \\ u(M,1) & u(M,2) & \dots & u(M,N) \end{bmatrix}$$

$$= u\left[\left(m - \frac{M}{2}\right)\Delta x, \tilde{y}, \tilde{z}, d + n\Delta t_s\right] \quad \text{for} \quad m = 1, 2, ..., M, \quad n = 1, 2, ..., N. \tag{6}$$

In order to smoothly extract from such matrix only the complex array, representing the spatial field distribution along $x$, we have to chose a time sampling frequency $f_s = 1/\Delta t_s$ equal to an integer multiple of $4f_0$. This condition is required because if:

$$f_s = 4kf_0, \qquad \text{and} \qquad \Delta t_s = \frac{1}{f_s} = \frac{1}{4kf_0} \tag{7}$$

then for each $x$, the time instants where the field is sampled, are $t_n = n\Delta t_s$, so that the "in phase" and "in quadrature" components have phases given by:

$$\omega_0 t_n = \frac{2\pi f_0 n}{4kf_0} = \frac{2\pi}{4k} n \qquad \text{(Phase)},$$

$$\omega_0 t_n - \frac{\pi}{2} = \frac{2\pi}{4k}(n-k) \qquad \text{(Quadrature)}$$

or, with reference to matrix $\mathbf{u}$, for a specific (space) row $m$, the time components corresponding to indexes $n$ and $n - k$.

Therefore, once a starting time $\tilde{t} = \tilde{n}\Delta t_s$ is chosen such that the field amplitude remains sufficiently steady in the previous $k\Delta t_s$ seconds, we evaluate the complex field at $y = \tilde{y}$ and $z = \tilde{z}$ through the complex array $\mathbf{U}$ whose components are:

$$U(m) = u(m, \tilde{n}) + ju(m, \tilde{n} - k) \qquad \text{for} \quad m = 1, 2, ..., M. \tag{8}$$

By repeating this procedure for several depth, a 2D complex representation of the field in space (e.g. $xz$ scan), can be extracted by the time domain data.

## 3. Results

The field distribution obtained with the method described above was first compared with the approximated expression of the space field distribution produced in the focal plane by a spherically focused circular transducer that can be found in the literature [11, 1, 12]. It is proportional to the so-called Airy distribution, given by:

$$u_{\text{Airy}} = \rho c \frac{u_0}{\lambda} \frac{\pi a^2}{R} \frac{2J_1(\xi)}{\xi}, \qquad \xi = \frac{2\pi a \rho'}{\lambda R}, \tag{9}$$

where $J_1$ indicates the first order Bessel function, and the meaning of the symbols is the following one:

- $\rho$ density of the propagating medium (Kg/m$^3$),
- $c$ sound velocity in the propagating medium (m/s),
- $\lambda$ wavelength in the propagating medium (m),
- $a$ aperture radius (m),
- $R$ geometrical focus (m),
- $\rho'$ radial distance off-axis (m).

As specified in the previous section, since we do not have a quantitative value of the transducer velocity, our interest is for the qualitative field distribution. Therefore only a normalized version of Eq. (9) can be considered and compared with the corresponding normalized field obtained from the simulation procedure. With reference to the cartesian reference shown in Fig. 1:

$$u'_{\text{Airy}}(x,y) = \frac{J_1(\xi(x,y))}{\xi(x,y)}, \qquad \xi(x,y) = \frac{2\pi a}{\lambda R}\sqrt{x^2+y^2}. \tag{10}$$

The data used for the comparison were the same as indicated for Fig. 2 ($a = 4\,\text{mm}$, $R = 30\,\text{mm}$, $c = 1500\,\text{m/s}$, $\lambda = c/f_0 = 1500/8 \cdot 10^6 = 187.5\,\mu\text{m}$) over the $x$ axis.

This expression is valid for CW excitation, hence the simulation procedure was performed with an excitation pulse long enough to produce a steady field after a transition period. In Fig. 3 a a gray level image of the transient field at $z = 30\,\text{mm}$ is shown, where two lines indicate the phase and quadrature times, chosen after nine burst pulses, in order to have a fully developed spatial field.

In Fig. 3 b the function represented by Eq. (10) has been plotted (dotted line) for $y = 0$ and $x$ ranging from $-6$ to 6 mm. In the same figure the continuous line indicates the normalized field amplitude obtained by processing the time domain data of Fig. 3 a. The strong agreement between the two curves make them almost not distinguishable.

The phase behavior obtained from the analytical Airy distribution is shown in Fig. 3 c with a dotted line. It exhibits a flat null behavior with alternate jumps from 0 to $\pi$ for each zero of the field amplitude. Differently from the extremely good agreement between the simulated and analytical amplitudes, the phase variation originated by the simulation differs evidently from the analytical one. The geometrical focus, where such behavior has been calculated, is in fact farer from the aperture respect to the true focus F, where the maximum amplitude holds and the phase distribution is flat. In general [5, 13] the phase plot of a focused beam is concave with concavity oriented away from the transducer

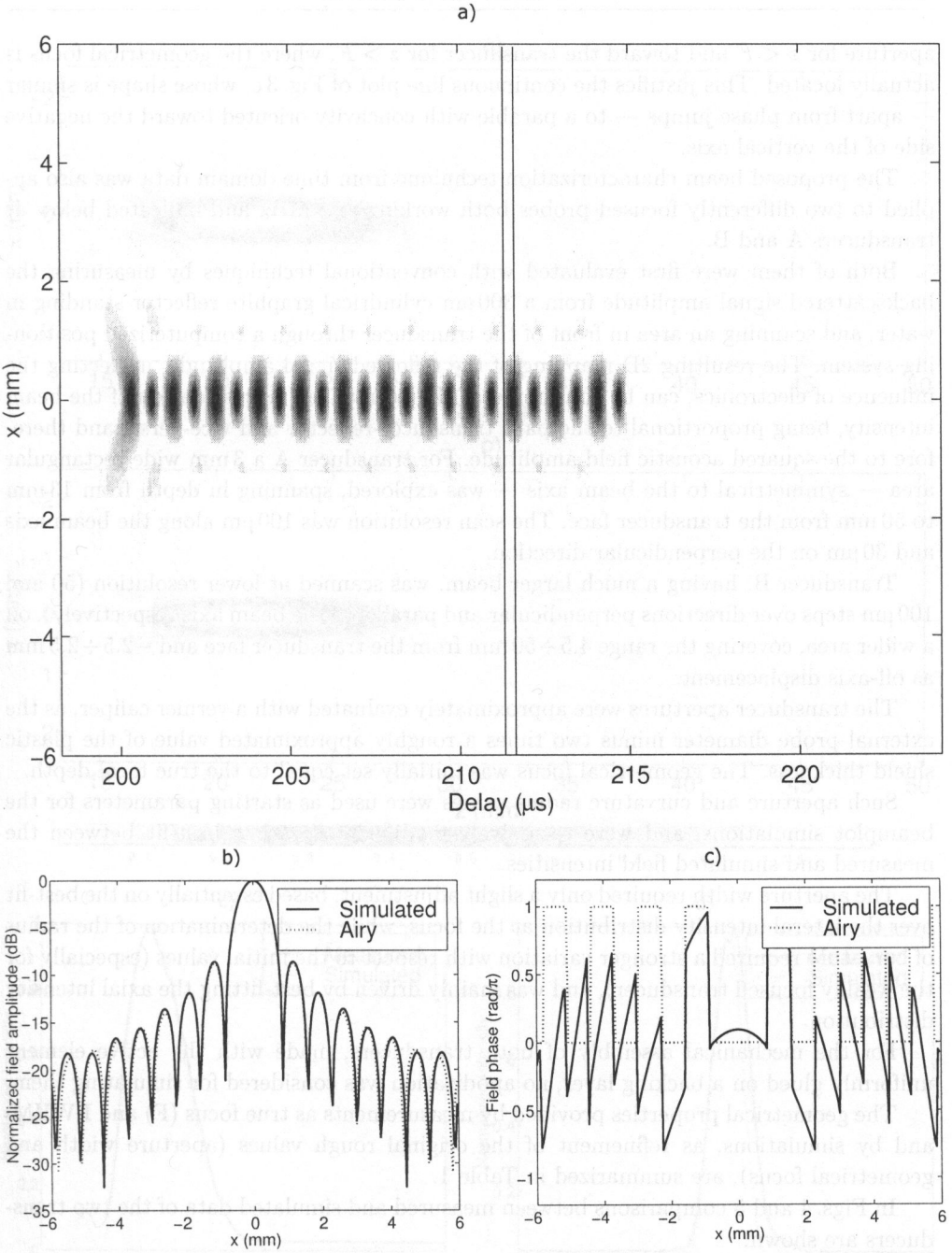


Fig. 3. Simulation of the field generated at $z = 30$ mm by the same transducer of Fig. 2 excited with an 8 MHz burst composed by 12 cycles; a) time-space representation of the field. The vertical lines represent the Phase and Quadrature sampling instants. b) Field amplitude module. c) Field phase.

aperture for $z < F$ and toward the transducer for $z > F$, where the geometrical focus is actually located. This justifies the continuous line plot of Fig. 3 c, whose shape is similar — apart from phase jumps — to a parable with concavity oriented toward the negative side of the vertical axis.

The proposed beam characterization technique from time-domain data was also applied to two differently focused probes both working at 8 MHz and indicated below as transducers A and B.

Both of them were first evaluated with conventional techniques by measuring the backscattered signal amplitude from a 300 μm cylindrical graphite reflector standing in water, and scanning an area in front of the transducer through a computerized positioning system. The resulting 2D mapping of the reflected signal amplitude, neglecting the influence of electronics, can be considered as the normalized representation of the beam intensity, being proportional to the path transducer-reflector and vice-versa, and therefore to the squared acoustic field amplitude. For transducer A a 3 mm wide rectangular area — symmetrical to the beam axis — was explored, spanning in depth from 13 mm to 50 mm from the transducer face. The scan resolution was 100 μm along the beam axis and 30 μm on the perpendicular direction.

Transducer B, having a much larger beam, was scanned at lower resolution (50 and 100 μm steps over directions perpendicular and parallel to the beam axis respectively), on a wider area, covering the range $4.5 \div 50$ mm from the transducer face and $-2.5 \div 2.5$ mm as off-axis displacement.

The transducer apertures were approximately evaluated with a vernier caliper, as the external probe diameter minus two times a roughly approximated value of the plastic shield thickness. The geometrical focus was initially set equal to the true focal depth.

Such aperture and curvature radius values were used as starting parameters for the beamplot simulations, and were recursively modified to reach a best-fit between the measured and simulated field intensities.

The aperture width required only a slight adjustment, based essentially on the best-fit over the lateral intensity distribution at the focus, while the determination of the radius of curvature required a stronger variation with respect to the initial values (especially for the weakly focused transducer), and was mainly driven by best-fitting the axial intensity distribution.

For the mechanical assembly of both transducers, made with the active element uniformly glued on a backing layer, no apodization was considered for simulating them.

The geometrical properties provided by measurements as true focus (F) and FWHM, and by simulations, as refinement of the original rough values (aperture width and geometrical focus), are summarized in Table 1.

In Figs. 4 and 5 comparisons between measured and simulated data of the two transducers are shown.

Figure 4 reports data related to the transducer A. The measured and simulated 2D beam intensity plot after normalization have been reported (Fig. 4 a and 4 b, respectively). The strong qualitative agreement between them is confirmed by the variation of the normalized field with distance on the beam axis (Fig. 4 c), and with lateral displacement at the true focus (Fig. 4 d).

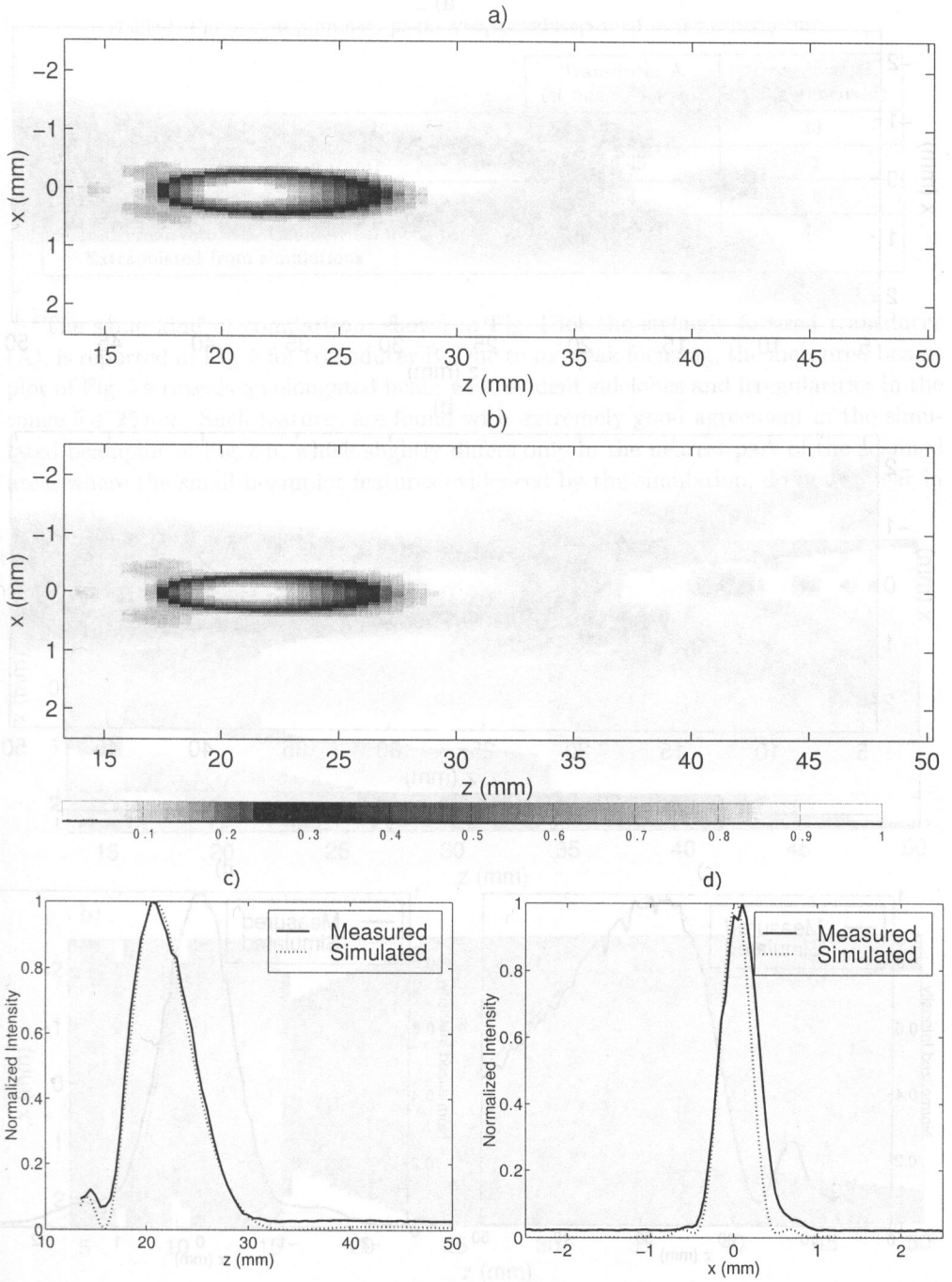


Fig. 4. Transducer A (strongly focused). 2D plot of the beam intensity a) measured; b) simulated; beam intensity along the $z$ axis (c), and along the $x$ axis at the focus (d).

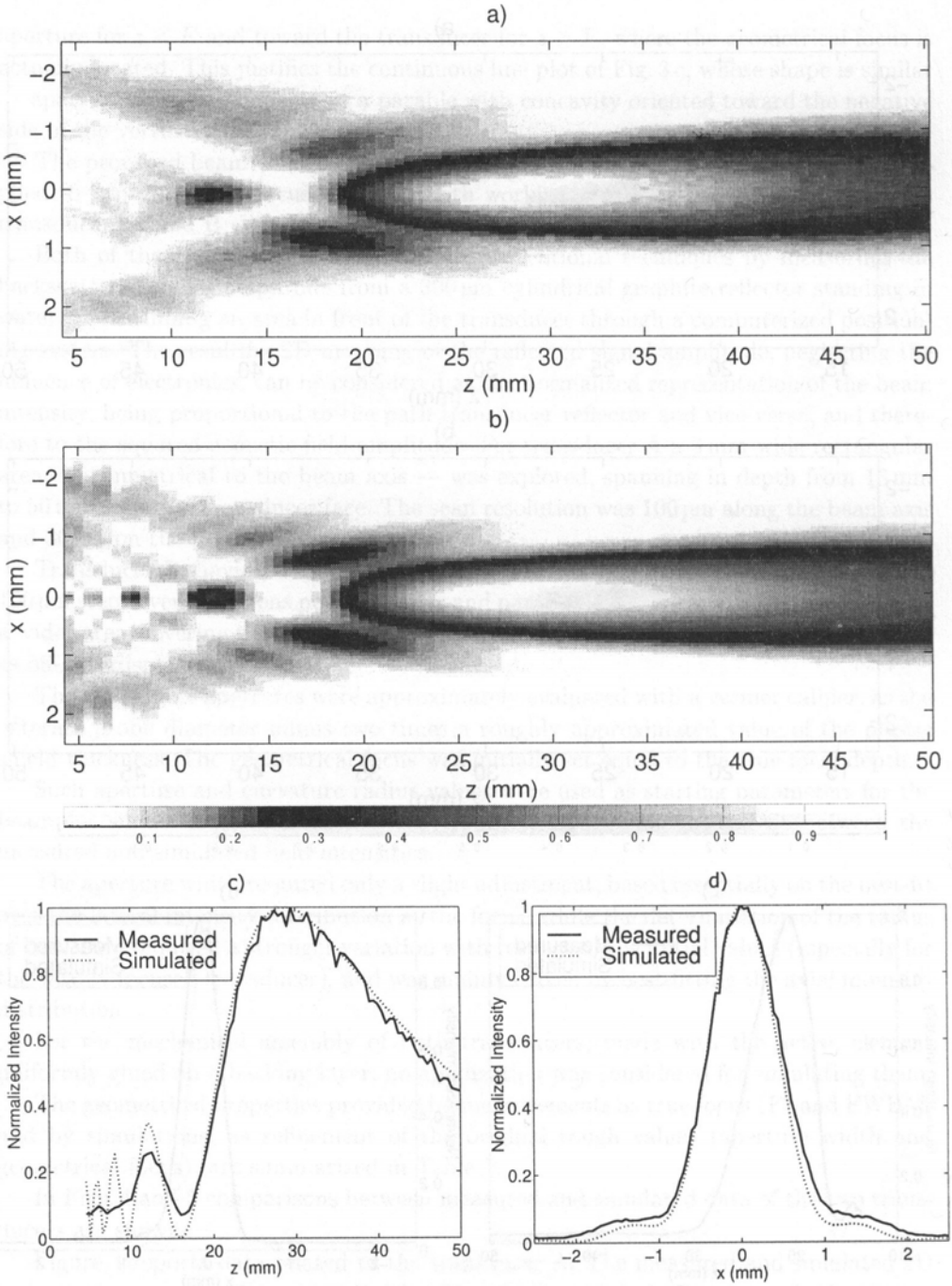


Fig. 5. Transducer B (weakly focused). 2D plot of the beam intensity a) measured; b) simulated; beam intensity along the $z$ axis (c), and along the $x$ axis at the focus (d).

**Table 1.** Parameters summary of the two transducers used in the experiments.

| | Transducer A (strongly focused) | Transducer B (weakly focused) |
|---|---|---|
| F or True focus (mm) — Measured | 20.75 | 30 |
| FWHM or −6 dB beamwidth (mm) — Measured | 0.45 | 1 |
| Diameter (mm) — Extrapolated from simulations | 9.4 | 6 |
| Radius of curvature or Geometrical focus (mm) — Extrapolated from simulations | 21.6 | 46 |

The same kind of comparison, shown in Fig. 4 for the strongly focused transducer (A), is reported in Fig. 5 for transducer B. Due to its weak focusing, the measured beamplot of Fig. 5 a reveals an elongated beam with evident sidelobes and irregularities in the range $5 \div 25$ mm. Such features are found with extremely good agreement in the simulated beamplot of Fig. 5 b, which slightly differs only in the nearest part of the scanned area, where the small beamplot features evidenced by the simulation, do not appear in

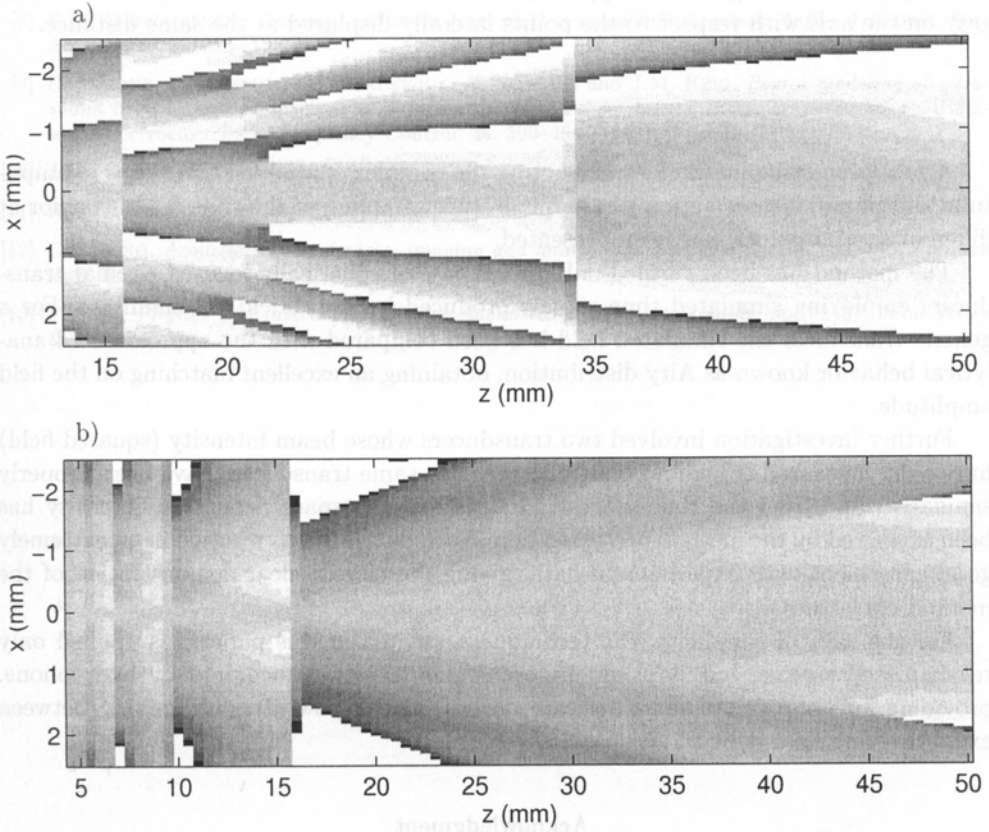


Fig. 6. Phase distributions of both transducers from the complete fields originating Figs. 4 b and 5 b; a) Transducer A, $F = 20.75$ mm; b) Transducer B, $F = 30$ mm. In the gray level scale $-\pi$ corresponds to white and $+\pi$ to black. The absence of any phase unwrapping involves abrupt white-to-black transitions.

Fig. 5 a. This might be due to the 300 μm echogenic target used to obtain the measured beamplot. It was wider than $\lambda$ (187.5 μm in 20° pure water), being actually a reflector rather than a scatterer, and therefore capable of producing an intrinsic smoothing of the beamplot which could have hidden some tiny details. The qualitative agreement of the two beamplots of Figs. 5 a and 5 b is confirmed by the simulated and measured behaviors of the field intensity along $z$-axis (Fig. 5 c), and along $x$-axis at the focal distance (Fig. 5 d).

From the complete fields originating such nicely matched beamplots, the phase fields were calculated and shown in Fig. 6 with a gray level scale where $-\pi$ corresponds to white and $\pi$ to black. The absence of any phase unwrapping involves abrupt white-to-black transitions visible in both images of Fig. 6.

Transducer A (Fig. 6 a) exhibits a stronger phase bending in comparison with transducer B (Fig. 6 b) as shown by the higher number of white-to-black transitions present in Fig. 6 a. In both cases near the beam axis the phase curvature is positive for $z < F$ as shown for a given distance by a gray level lighter on the axis rather than off-axis. Looking at the two figures the opposite situation is evident for $z > F$, with a darker gray on the axis with respect to the points laterally displaced at the same distance.

## 4. Conclusions

A new processing method for extracting the complex spatial field, in terms of amplitude and phase, from a proper phase-quadrature sampling of the time field behavior at different spatial points, has been presented.

The method has been verified only in the case of spherically focused circular transducers employing simulated time signals produced by the "Field II" simulator. For a generic transducer the simulated field has been compared with the approximated analytical behavior known as Airy distribution, obtaining an excellent matching on the field amplitude.

Further investigation involved two transducers whose beam intensity (squared field) have been measured trough a point-reflector. The same transducers have been properly simulated, and from the time-space field variation, the space dependent intensity has been extracted by the method presented here. Such distributions resulted in an extremely good agreement with experimental data, giving therefore a clear demonstration of the method correctness.

For the sake of simplicity, the technique presented in this paper was applied only to simulated signals, but it would be applicable to signals acquired by hydrophone, providing an appropriate sampling rate, and a precise (low-jitter) triggering between excitation and field data acquisition.

## Acknowledgment

The authors wish to thank Professor PIERO TORTOLI, from the Electronic Engineering Dept. of the University of Florence, for useful discussions.

## References


[1] J.W. HUNT, M. ARDITI and F.S. FOSTER, *Ultrasound transducers for pulse echo medical imaging*, IEEE Trans. on Biomed. Eng., **30**, 453–481 (1983).

[2] P.J. FISH, *Doppler methods*, [in:] Physical Principles of Medical Ultrasonics, 350–363, C.R. HILL [Ed.], Ellis Horwood, Chichester, UK 1986.

[3] O.W. ATA and P.J. FISH, *Effect of deviation from plane wave conditions on the Doppler spectrum from an ultrasonic blood flow detector*, Ultrasonics, **29**, 395–403 (1991).

[4] J.D. AINDOW and R.C. CHIVERS, *Measurement of the phase variation in an ultrasonic field*, J. Phys. E: Sci. Instrum., **15**, 83–86 (1982).

[5] G. GUIDI and S. FALTERI, *Phase measurement of acoustic fields based on a moving target*, IEEE Transactions on Ultrasonics, Ferroelectrics & Frequency Control, **46**, 679–689 (1999).

[6] J.A. JENSEN and N.B. SVENDSEN, *Calculation of pressure fields from arbitrarily shaped, apodized, and excited ultrasound transducers*, IEEE Transactions on Ultrasonics, Ferroelectrics & Frequency Control, **39**, 262–267 (1992).

[7] G.E. TUPHOLME, *Generation of acoustic pulses by baffled plane pistons*, Matematika, **16**, 209–224 (1969).

[8] P.R. STEPHANISHEN, *Transient radiation from pistons in an infinite planar baffle*, J. Acoust. Soc. Am., **77**, 1629–1638 (1971).

[9] E. MAIONE, P. TORTOLI, G. ŁYPACEWICZ, A. NOWICKI and J.M. REID, *Pspice modeling of ultrasound transducers: comparison of software models to experiments*, IEEE Transactions on Ultrasonics, Ferroelectrics & Frequency Control, **46**, 399–406 (1999).

[10] J.W. GOODMAN, *Introduction to Fourier optics*, pp. 33–34, McGraw-Hill, New York 1968.

[11] H.T. O'NEIL, *Theory of focusing radiators*, J. Acoust. Soc. Am., **21**, 126–516 (1949).

[12] G.S. KINO, *Acoustic waves: devices, imaging and analog signal processing*, pp. 182–186, Prentice Hall, Englewood Cliffs, 1987.

[13] P. FISH, *Physics and instrumentation of diagnostic medical ultrasounds*, pp. 32–37, John Wiley & Sons, 1990.